 Bull. Chem. Soc. Jpn., 74, 1467–1475 (2001)

Static and Dynamic Stereochemistry of *N*-Alkyl- and *N*,*O*-Dialkyl-*N*-9-triptycylhydroxylamine Derivatives

Gaku Yamamoto,* Fusako Nakajo, Naoka Endo, and Yasuhiro Mazaki

Department of Chemistry, School of Science, Kitasato University, Kitasato, Sagamihara, Kanagawa 228-8555

(Received February 22, 2001)

Stereochemistry of *N*-9-triptycylhydroxylamine and its *N*-alkyl and *N*,*O*-dialkyl derivatives was studied. X-ray crystallographic analysis of *N*,*O*-diethyl-*N*-9-triptycylhydroxylamine revealed (a) the chiral nature of the molecule, (b) an almost tetrahedral geometry of the nitrogen atom, and (c) a nearly eclipsing arrangement of the O–Et bond with the nitrogen lone-pair orbital. In solution, enantiomerization takes place rapidly at room temperature on the NMR time scale but slows down at low temperatures. The stereomutation proceeds by way of two processes, "R-passing," and "O-passing," in which the alkyl (R) and oxy (OH or OR) groups attached to the nitrogen atom, respectively, pass over a benzene ring, accompanied by nitrogen inversion and partial rotation of the N–O bond. The energy barriers to these processes were obtained by dynamic NMR spectroscopy.

Static and dynamic stereochemistry of compounds with nitrogen–heteroatom bonds, such as hydrazines, hydroxylamines, sulfenamides, and aminophosphines, have long been subjects of extensive investigation.[1,2,3] Conformation around the nitrogen–heteroatom bond is governed by interaction between the lone pair electrons on the nitrogen and on the adjacent heteroatom. The interaction not only affects stable conformations but also increase barriers to conformational interconversion, which involves inversion at the nitrogen atom and rotation about the nitrogen–heteroatom bond.

The most stable molecular geometry of hydroxylamine is known to be the one in which the nitrogen atom is sp^3-hybridized and the O–H bond is anticlinal to the N–H bonds and thus eclipsed with the sp^3 lone-pair orbital on the nitrogen atom (Scheme 1).[1] This geometry is favored because the electrostatic repulsion between the lone pairs on the nitrogen and the oxygen is minimized.[4] This situation is in sharp contrast to that in methanol, where a staggered conformation is favored (Scheme 1). The most stable conformation in hydroxylamines with simple alkyl substituents is shown by **A** in Scheme 2,[1] which is chiral when the nitrogen substituents R^1 and R^2 are different. It has been accepted that interconversion between **A** and its enantiomer $\bar{\mathbf{A}}$ takes place with successive nitrogen inversion (Inv) and N–O bond rotation (Rot) by way of less stable conformations **B** and $\bar{\mathbf{B}}$ with the O–R bond antiperiplanar to the nitrogen lone-pair. The energy barriers to the interconversion are generally in the range that is accessible by dynamic NMR spectroscopy, and many studies on various types of hydroxylamine derivatives have been reported.[1,2,3] In several cases it is rather easy to determine which of the two processes has a higher barrier and is rate-determining, but there are many cases where that is still ambiguous.

We have long been interested in the stereochemistry of triptycene derivatives, because the triptycene skeleton has a unique and highly symmetric geometry and in derivatives carrying a substituent at the bridgehead position (9-position) the bridgehead-to-substituent bond generally has an unusually high energy barrier to internal rotation.[5] We have recently studied stereodynamics of derivatives with a nitrogen substituent at the bridgehead: *N*,*N*-dialkyl-9-triptycylamines,[6] *N*-phenyl-9-triptycylamines,[7] and *N*-alkyl-*N*-9-triptycylacetamides.[8] In the course of these studies we have been interested in the stereochemistry of hydroxylamine derivatives carrying the 9-triptycyl (Tp) group at the nitrogen atom; how the bulky Tp group affects the molecular geometries and energy barriers to

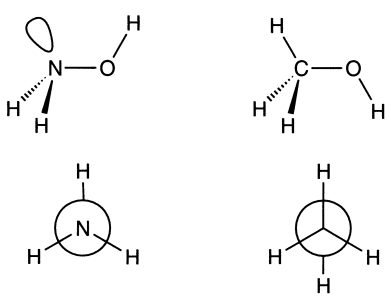

Scheme 1.

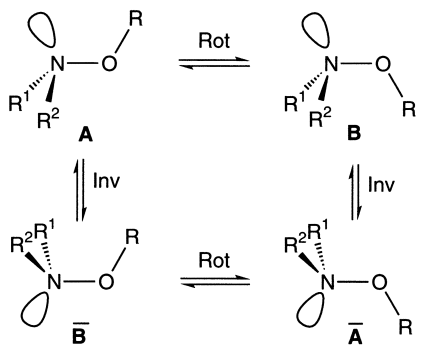

Scheme 2.

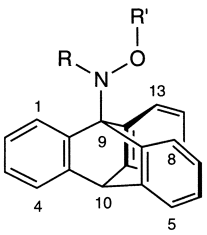

	R	R'
1	H	H
2	C_2H_5	H
3	C_2H_5	CH_3
4	C_2H_5	C_2H_5
5	CH_3	H
6	CH_3	CH_3
7	CH_3	C_2H_5

Chart 1.

stereomutation. Here we report static and dynamic stereochemistry of *N*-9-triptycylhydroxylamine (**1**) and several *N*-alkyl and *N*,*O*-dialkyl derivatives **2**–**7** (Chart 1).[9]

Results and Discussion

Syntheses. *N*-9-Triptycylhydroxylamine (**1**) was obtained by reduction of 9-nitrotriptycene with $LiAlH_4$ as reported by Theilacker and Beyer.[10] As the only derivative of **1** so far known, the hydriodide of *N*-methyl-*N*-9-triptycylhydroxylamine (**5**) was also reported by Theilacker and Beyer.[10] They claimed to have obtained **5**·HI by heating **1** with methyl iodide at 250 °C in a sealed tube, but the characterization was based solely on elemental analysis, and they did not characterize **5** itself. We repeated the reported procedure and tried to obtain **5** as a neutral form, but could not characterize **5** even by spectroscopic methods. Thus we attempted another route to **5**, i.e., the reaction of **1** with methyl trifluoromethanesulfonate (triflate) in the presence of pyridine, which was proved successful. That the methylation took place at the nitrogen atom and not at the oxygen atom was spectroscopically confirmed: ν_{OH} at 3580 cm^{-1} in $CDCl_3$ and the *N*-methyl signal at $\delta_H = 3.82$ and $\delta_C = 47.1$ in $CDCl_3$. *N*-Ethyl-*N*-9-triptycylhydroxylamine (**2**) was similarly prepared by reaction of **1** with ethyl triflate. Attempts to prepare the *N*-benzyl and *N*-isopropyl derivatives have so far been unsuccessful.

N,*O*-Dialkyl compounds were synthesized by deprotonation of the OH group with a strong base followed by alkylation with triflates. Thus compounds **3** and **4** were prepared by deprotonating **2** with butyllithium and then treating with methyl and ethyl triflates, respectively. In the case of **5**, deprotonation with butyllithium was complicated by lithiation at a peri position of the triptycene skeleton, and thus potassium *t*-butoxide was used instead, affording **6** and **7**.

X-ray Crystallographic Analysis of Compound 4. In order to have insights into the molecular geometries that *N*-9-triptycylhydroxylamines would have in the crystalline state, we attempted X-ray crystallographic analysis of an appropriate derivative. The *N*,*O*-diethyl compound **4** gave suitable single crystals and thus was subjected to the X-ray analysis. Two independent molecules are in a unit cell, but their molecular structures are quite similar to each other. The perspective drawings for one of them (Molecule **A**) are given in Fig. 1. Selected bond lengths, bond angles, and torsion angles are compiled in Table 1.

The geometry around the nitrogen atom is almost tetrahedral; the sum of the bond angles around the nitrogen atom is 326.2°, which is close to the 328.5° value expected for a tetrahedral geometry. The conformation about the Tp–N bond is

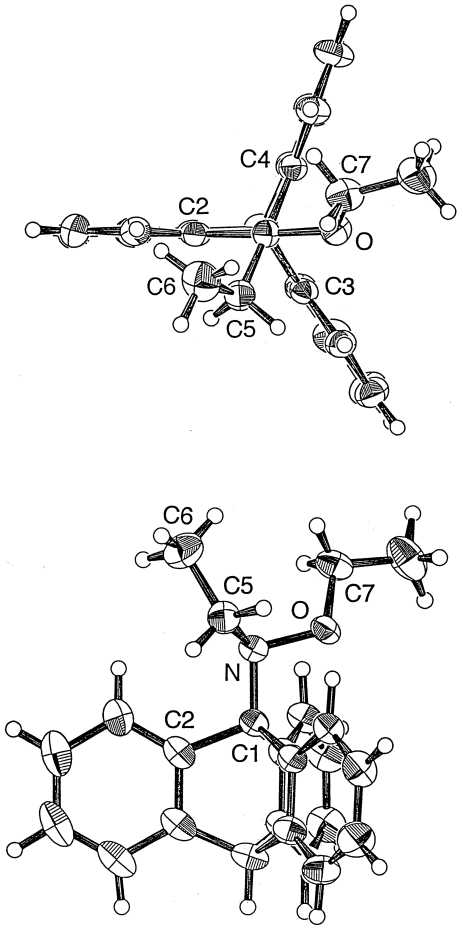

Fig. 1. Perspective drawings of the molecular structure of molecule **A** of compound **4**.

completely staggered, as shown by the dihedral angles around the C1–N bond in Table 1. If the geometry around the N–O moiety predicted for simple hydroxylamine derivatives (Conformation **A** in Scheme 2) is assumed to hold in **4**, the dihedral angles C1–N–O–C7 and C5–N–O–C7 should be 120 and −120°, respectively. Actually the values of ca. 148 and −90°, respectively, are observed in **4** (Table 1), which deviate by ca. 30° from the "ideal" values. The "ideal" geometry would cause significant steric repulsion between the *O*-methylene moiety and the proximal benzene ring of the Tp group, and the N–O bond would rotate by ca. 30° so as to relieve the repulsion. This deformation would in turn cause the steric repulsion between the *O*-methylene and the methyl group of the *N*-ethyl group, which would result in the tilting of the methyl group from the staggered conformation, affording the C1–N–C5–C6 angle of −144.2° (Fig. 1 and Table 1).

Molecular Mechanics Calculations. In order to supplement the X-ray crystallographic data, molecular mechanics calculations were performed for compound **4** using the MM3 program. As the program does not contain the force field parameters for the hydroxylamine moiety, several parameters were added; these are shown in the Experimental section. Geometrical parameters obtained for the most stable conformation of **4** are included in Table 1. The results show that the calculation excellently reproduces the X-ray geometry in spite

Table 1. Selected Bond Lengths, Bond Angles, and Torsion Angles around the Hydroxylamine Moiety in Molecules **A** and **B** of Compound **4** Obtained by X-ray Crystallography and Those by Molecular Mechanics Calculations (MM3)[a)]

	Molecule **A**	Molecule **B**	MM3
N–O	1.460(2)	1.458(2)	1.457
N–C1	1.474(2)	1.474(2)	1.476
N–C5	1.495(2)	1.488(2)	1.476
O–C7	1.428(2)	1.426(2)	1.422
C1–C2	1.550(2)	1.543(2)	1.534
C1–C3	1.548(2)	1.552(2)	1.538
C1–C4	1.546(2)	1.544(2)	1.531
O–N–C1	104.4(1)	104.7(1)	108.0
O–N–C5	107.4(1)	107.2(1)	108.4
C1–N–C5	114.4(1)	114.3(1)	115.2
N–O–C7	110.7(1)	111.1(1)	112.6
N–C1–C2	111.7(1)	111.5(1)	112.9
N–C1–C3	117.2(1)	117.0(1)	114.5
N–C1–C4	112.6(1)	113.0(1)	113.0
N–C5–C6	112.4(1)	112.7(1)	112.9
C1–N–O–C7	148.9(1)	147.8(1)	148.2
C5–N–O–C7	−89.3(1)	−90.4(1)	−86.3
O–N–C1–C2	−177.5(1)	−178.4(1)	−177.0
O–N–C1–C3	59.5(1)	58.3(1)	59.2
O–N–C1–C4	−63.8(1)	−64.5(1)	−62.1
C5–N–C1–C2	65.4(2)	64.7(2)	61.7
C5–N–C1–C3	−57.5(2)	−58.3(2)	−62.1
C5–N–C1–C4	179.2(1)	178.6(1)	176.6
C1–N–C5–C6	−144.2(2)	−145.2(2)	−143.1
O–N–C5–C6	100.5(2)	99.3(2)	95.0

a) The numbering is shown in Fig. 1. Bond lengths are in Å and angles are in °.

of the poor parametrizations for the hydroxylamine moiety. This suggests that the molecular geometry is mainly governed by steric interactions in the molecule rather than the electronic interactions within the hydroxylamine moiety, and also that the molecule will adopt a conformation in solvents of low polarity similar to that in the crystalline state.

The molecular mechanics calculations were also performed for compounds **2** and **6** in some detail. For each compound, the most stable conformation was found to be the one schematically shown in Fig. 2 (vide infra). The calculated Tp–N–O–R′ dihedral angles are 129.0° and 151.0° for **2** and **6**, respectively. A second, less stable conformation was found around the N–O bond for both compounds. The second conformer for **2** is 1.4 kJ mol^{-1} less stable than the most stable one and the Tp–N–O–H angle is −18.6°, while that for **6** is 20.5 kJ mol^{-1} less stable than the global minimum, the Tp–N–O–CH_3 angle being −68.0°. The geometries and energies calculated for conformers of **2** may be less reliable, because conformation of the N–O–H moiety is less susceptible to steric interactions and thus more dependent on the electronic nature of the moiety, which is hard to adequately reproduce in the present calculations. Anyway, the calculated geometry of the most stable conformation for **2** and **6** is consistent with the one deduced from the NOE experiments, as described below.

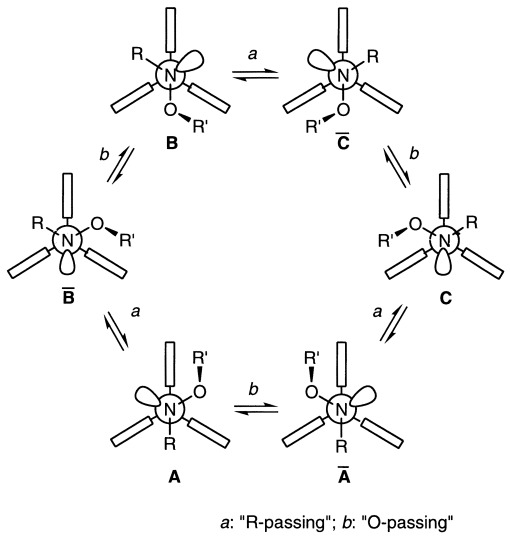

Fig. 2. Conformations and interconversion processes of a *N*-9-triptycylhydroxylamine derivative.

Conformations and NMR Assignments in Solution. ^{1}H NMR spectra of compounds **1**–**7** in CD_2Cl_2 at ambient temperature reveal that dynamic processes, bond rotations and nitrogen inversion, take place rapidly on the NMR time scale. Three benzene rings of the Tp moiety are magnetically equivalent, although the signals ascribed to the peri-protons at the 1-, 8-, and 13-positions of the Tp skeleton are somewhat broadened in any compound. Signals of the ethyl groups in compounds **2**, **3**, **4**, and **7** appear as an A_2X_3 pattern, reflecting the mutual equivalence of the two methylene protons.

Upon lowering the temperature, both the methylene and the aromatic proton signals broaden, split, and resharpen, reflecting the slow-down of stereomutation. At ca. −70 °C stereomutation is almost frozen on the NMR time scale in **2**–**7**; three benzene rings of the Tp skeleton are mutually nonequivalent and the signals of three peri-protons are separately observed. Each ethyl group in **2**, **3**, **4**, and **7** affords an ABX_3-pattern signal; the methylene protons are diastereotopic and anisochronous. Stereomutation in compound **1** is not yet completely frozen even at −90 °C, although three broad signals due to the peri-protons are separately observed at this temperature.

It will be reasonable to presume that the conformation of the hydroxylamine moiety in compounds **1**–**7** in solution is similar to the one found in the crystalline state for **4**. Thus the Newman projections in Fig. 2 schematically show conformations adopted by these compounds. Conformations **A**, **B**, and **C** are equivalent and can be distinguished only when the three benzene rings are assumed to be distinguished. Conformations $\bar{\mathbf{A}}$, $\bar{\mathbf{B}}$, and $\bar{\mathbf{C}}$ are the enantiomeric forms of **A**, **B**, and **C**. Below ca. −70 °C, molecules of **2**–**7** are almost frozen in one of these conformations on the NMR time scale.

Nuclear Overhauser effect (NOE) experiments at temperatures where the exchange is sufficiently slow enabled the chemical shift assignments of the peri-protons of the Tp moiety as well as the methylene protons of the ethyl groups.

As a typical example, Fig. 3 shows the aromatic region spectrum of compound **2** in CD_2Cl_2 at −72 °C. Six one-proton signals are explicitly observed at lower field together with

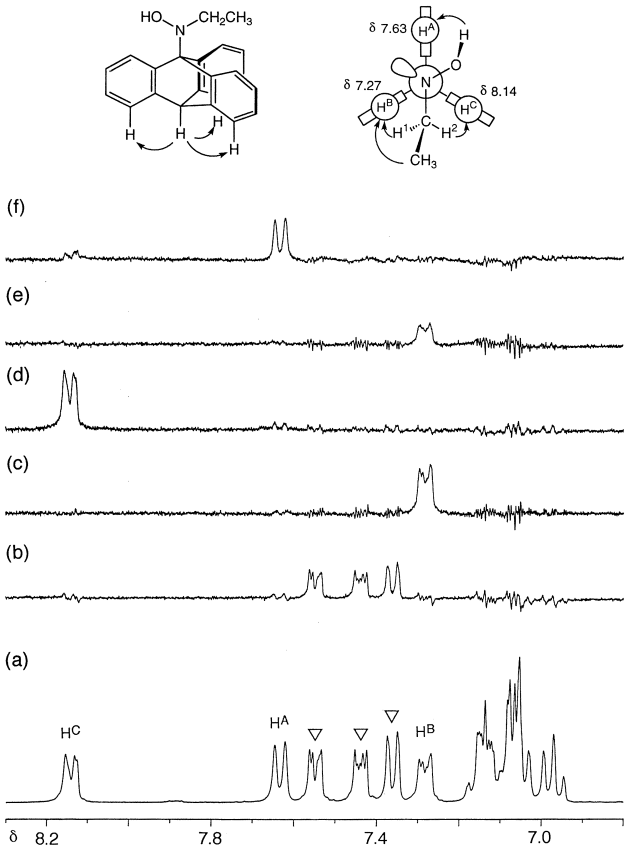

Fig. 3. NOE results of compound **2** at −72 °C in CD_2Cl_2. (a) The normal spectrum, and NOE difference spectra upon irradiation of (b) the bridgehead proton (10-H), (c) the methylene proton at δ 3.81, (d) the methylene proton at δ 4.13, (e) the methyl protons, and (f) the OH proton.

overlapping signals for six protons at higher field. The three signals marked with the triangle symbols are assigned to the protons at 4-, 5-, and 16-positions on the basis of NOE upon irradiation of 10-H (ca. 10% enhancement). Irradiation of the higher-field methylene proton at δ 3.81 enhances the signal at δ 7.27 by 13%, while irradiation of the lower-field methylene proton at δ 4.13 enhances the signal at δ 8.14 by 15%. The results indicate that these signals are reasonably assigned to H^B and H^C flanking the ethyl group. Irradiation of the methyl protons enhances the signal at δ 7.27 by 6%, and irradiation of OH enhances the third peri-proton signal at δ 7.63 by 9%, which is unambiguously assigned to H^A. The individual assignments of H^B and H^C come from the following reasonings. Firstly, the steric repulsion between the methyl and OH groups would tilt the methyl group toward H^B as revealed by the MM3 calculations, and therefore the signal at δ 7.27 should be assigned to H^B. Secondly, the pathways shown in Fig. 2 do not exchange H^A and H^B in one step, and thus the reverse assignment, H^B at δ 8.14, contradicts the observed lineshape change discussed later.

The methylene protons of the *N*-ethyl group could also be assigned by these NOE results; the methylene proton (H^1) close to H^B appears at a higher field (δ 3.81) and the other one (H^2) close to H^C at a lower field (δ 4.13). If the methyl group is tilted toward H^B as discussed above, H^1 is expected to locate in the greater shielding region of the ring current effect of the nearby benzene ring and thus would appear at a higher field than H^2, which is consistent with the observation.

NOE experiments for compounds **3** and **4** allowed the assignments of the peri-protons in a similar manner to that mentioned above for compound **2**. Similarly, in the *N*-methyl compounds **5**–**7**, the signals enhanced upon irradiation of the *N*-methyl protons are assigned to H^B and H^C flanking the *N*-methyl group, and the one enhanced upon irradiation of OCH_2 or OCH_3 is assigned to H^A, the third peri-proton close to the OR group.

In any of compounds **2**–**7**, therefore, H^C flanked by R and OR′ appears at the lowest field (δ 8.0–8.2), H^B flanked by R and the nitrogen lone pair at the highest field (δ 7.25–7.45), and H^A flanked by OR′ and the lone pair at the intermediate region (δ 7.4–7.8). These assignments are essential to the lineshape analysis described in the following section.

For compound **1**, broad signals ascribed to the peri-protons appear at δ 7.32, 7.88, and 8.03 at −90 °C. The chemical shifts fall in the respective regions mentioned above and may be similarly assigned though NOE experiments were not made.

Dynamic NMR Spectroscopy. It is inferred that interconversion among the conformations shown in Fig. 2 takes place by way of two processes that are hereafter referred to as "R-passing" and "O-passing". In "R-passing" the alkyl group R passes over a benzene ring, e.g. **A** ⇄ $\overline{\mathbf{B}}$ in Fig. 2 and Scheme 3, while in "O-passing" the oxy group OR′ (OH or *O*-alkyl) passes over a benzene ring of the Tp moiety, e.g. **A** ⇄ $\overline{\mathbf{A}}$. Either process involves inversion at the nitrogen and partial rotation about the N–O bond, which may take place simultaneously or sequentially.

Rotation of the Tp–N bond without nitrogen inversion (i.e., direct interconversion among **A**, **B**, and **C** and among $\overline{\mathbf{A}}$, $\overline{\mathbf{B}}$, and $\overline{\mathbf{C}}$ in Fig. 2, and hereafter referred to as "rigid rotation") is concluded to have a higher energy barrier than the two processes mentioned above, according to the following reasoning: The exchange of the two methylene protons of an *N*- or *O*-ethyl group is caused only by the nitrogen inversion and never by the "rigid rotation". Actually the lineshape change of the ethyl methylene signal takes place concomitantly with that of the aromatic signals, indicating that the "rigid rotation" is not the lowest energy process. Therefore, the "rigid rotation" will not be considered hereafter.

As shown in Scheme 3, "R-passing" interchanges H^A and H^C, while "O-passing" interchanges H^B and H^C. Therefore the lineshape of the peri-proton signals is separately dependent on the rate constants of these two processes, and the two rate constants are independently obtained from lineshape analysis of

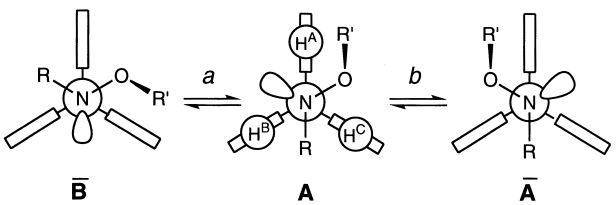

a: "R-passing"; *b*: "O-passing"

Scheme 3.

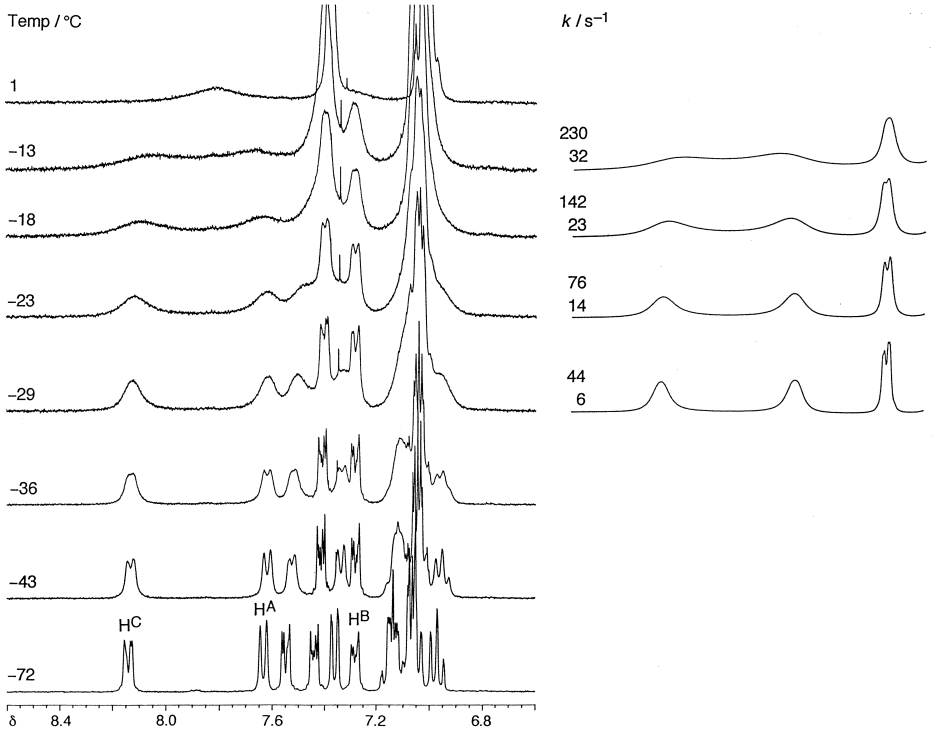

Fig. 4. The observed spectra of the aromatic region of compound **2** in CD_2Cl_2 at various temperatures (left) and the calculated spectra (right) with the best-fit rate constants for "R-passing" (upper) and "O-passing" (lower).

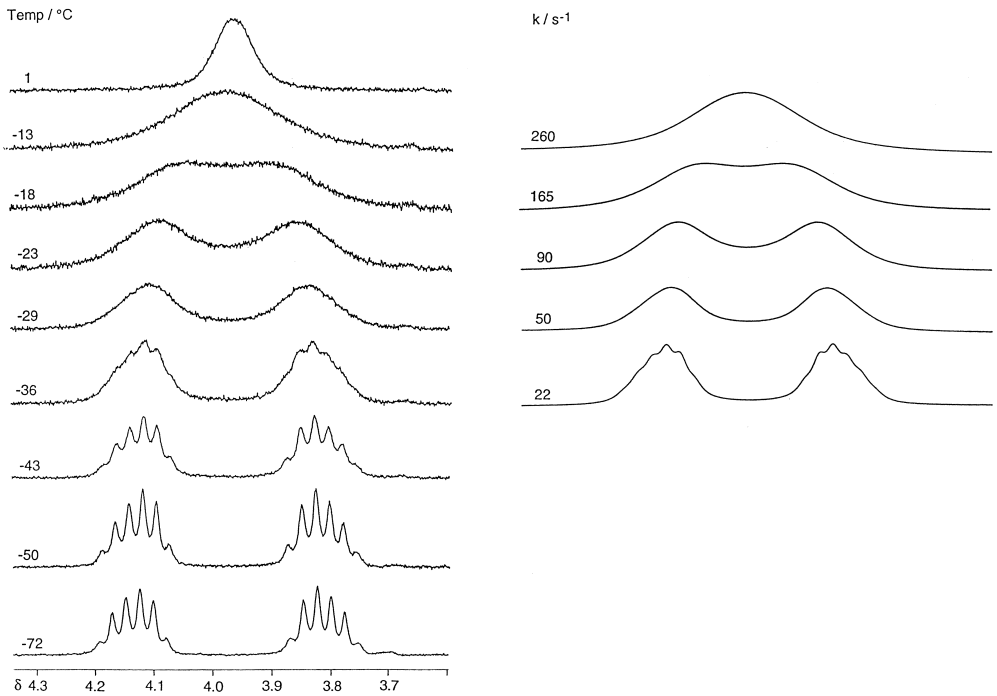

Fig. 5. The observed spectra of the methylene region of compound **2** in CD_2Cl_2 at various temperatures (left) and the calculated spectra with the best-fit rate constants (right).

the peri-proton signals. On the other hand, the methylene protons of an ethyl group, irrespective of whether it is attached to N or O, mutually exchange by either of the two processes, and thus lineshape analysis of the methylene signal affords a single rate constant which corresponds to the sum of the rate constants for the two processes.

The aromatic and the methylene proton spectra of compound **2** at several temperatures are shown in Figs. 4 and 5, respectively. As shown in Fig. 4, the signals assigned to H^A and H^C broaden at lower temperatures than the H^B signal upon rais-

Table 2. Rate Constants k (s^{-1}) and Free Energies of Activation $\Delta G^{\ddagger}$ (kJ mol^{-1}) at 250 K in CD_2Cl_2

Compd	R	R′	"O-passing"[a]		"R-passing"[a]		methylene[b]	
			k	$\Delta G^{\ddagger}$	k	$\Delta G^{\ddagger}$	k	$\Delta G^{\ddagger}$
2	Et	H	13 ± 2	55.5 ± 0.3	81 ± 6	51.7 ± 0.3	93 ± 5	51.4 ± 0.2
3	Et	Me	970 ± 100	46.6 ± 0.2	26 ± 4	54.1 ± 0.3	1000 ± 50	46.5 ± 0.2
4	Et	Et	980 ± 100	46.5 ± 0.2	22 ± 4	54.5 ± 0.3	1000 ± 50	46.5 ± 0.2
5	Me	H	110 ± 10	51.0 ± 0.2	53 ± 5	52.6 ± 0.2	—	—
6	Me	Me	860 ± 200	46.8 ± 0.4	3.1 ± 0.5	58.6 ± 0.4	—	—
7	Me	Et	1000 ± 200	46.5 ± 0.4	4.5 ± 0.5	57.7 ± 0.3	900 ± 50	46.7 ± 0.2

a) Obtained from the peri-proton signals. b) Obtained from the methylene signals.

ing the temperature from −72 °C. This suggests that interchange between H^A and H^C takes place more rapidly than that between H^B and H^C (or H^A). The lineshape of these signals can be simulated in terms of two rate constants, one for the H^A/H^C interchange (i.e., "R-passing") and the other for the H^B/H^C interchange (i.e., "O-passing"); H^A and H^B do not interchange in a single process as mentioned before. The calculated spectra at four temperatures between −29 and −13 °C obtained by the total lineshape analysis are also shown in Fig. 4, together with the best-fit rate constants. The rate constants at 250 K are obtained by interpolation to be 81 and 13 s^{-1} for "R-passing" and "O-passing", respectively, as compiled in Table 2 together with the free energies of activation at 250 K.

The lineshape of the methylene proton signal can be simulated using a single rate constant that represents the mutual exchange of the two protons. The best-fit calculated spectra at several temperatures are shown in Fig. 5. The rate constant at 250 K is calculated as 93 s^{-1} by interpolation. The value agrees well with the sum of the two rate constants (81 and 13 s^{-1}) obtained from the analysis of the aromatic signals mentioned just above.

For compounds **3** and **4**, temperature dependences of the ^1H NMR spectra in both the aromatic and the methylene regions are observed similarly as in the case of compound **2**. However, in these compounds, interchange of H^B and H^C takes place far faster than that of H^A and H^C; apparently, the H^B and H^C signals coalesce at ca. −35 °C, while the coalescence of the coalesced H^B/H^C signal with the H^A signal takes place above 0 °C. The rate constants and the free energies of activation at 250 K for the two processes are calculated as given in Table 2. Lineshape analysis of the methylene signals affords parameters very similar to those for "O-passing" obtained from the analysis of the aromatic signals. In compound **4** the *N*-methylene and *O*-methylene signals can be simulated with single rate constants.

Temperature dependence of the aromatic signals in the *N*-methyl compounds **5**–**7** was similarly analyzed and the kinetic parameters therefrom are also compiled in Table 2. The values, especially those for **6** and **7**, are less reliable, partly because of the severer overlap of the aromatic signals and partly because the temperature range in which the lineshape analysis is made is far from 250 K. The *O*-methylene signals in compound **7** give similar values of the kinetic parameters to those for "O-passing" from the aromatic signals, because "R-passing" is far slower.

As for the effects of substituents on the energy barriers to the two processes, several features are extracted from the data

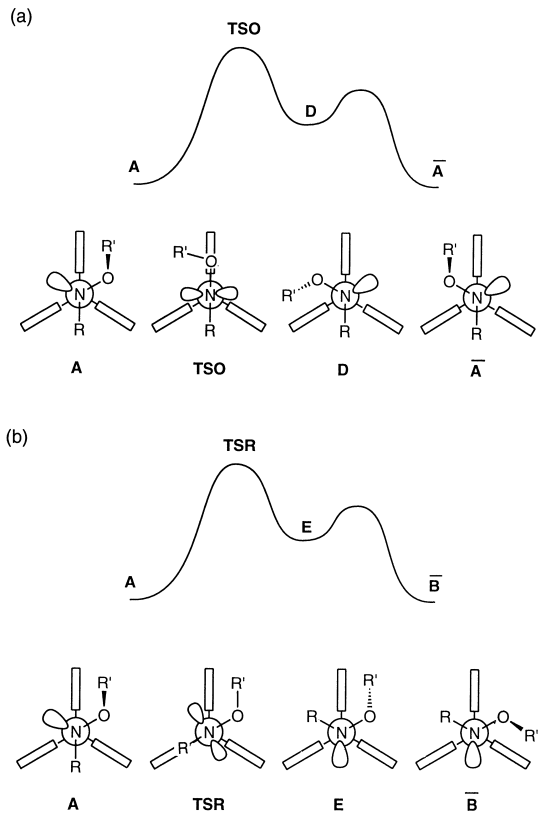

Fig. 6. Plausible schematic energy diagrams of "O-passing" (a) and "R-passing" (b).

in Table 2. (a) The "O-passing" barriers in the *N*,*O*-dialkyl derivatives **3**, **4**, **6**, and **7** are rather similar to each other and considerably lower than those in the *N*-alkyl derivatives **2** and **5**. (b) The "O-passing" barrier in the *N*-ethyl compound **2** is higher than that in the *N*-methyl one **5**. (c) The "R-passing" barriers in the *N*,*O*-dialkyl derivatives are higher than those in the corresponding *N*-alkyl derivatives; **3**, **4** > **2** and **6**, **7** > **5**. (d) The "R-passing" barriers in the *N*-methyl derivatives are higher than those in the corresponding *N*-ethyl derivatives; **5** > **2** and **6**, **7** > **3**, **4**. (e) The "R-passing" barriers are far higher than the "O-passing" barriers for the *N*,*O*-dialkyl derivatives, **3**, **4**, **6**, and **7**, while they are similar for the *N*-methyl compound **5** and even reversed for the *N*-ethyl compound **2**.

In order to understand these substituent effects, the following working hypothesis is constructed for the itineraries and the transition state structures of the rate processes. Plausible energy diagrams of the two processes are schematically shown

in Fig. 6.

In "O-passing", a molecule in the ground state conformation **A** will reach the rate-determining transition state (**TSO**), where the N–O bond eclipses one of the benzene ring of the Tp moiety, the nitrogen is planar, and the O–R′ bond lies periplanar to the p-type lone-pair orbital on the nitrogen in order to minimize the lone-pair/lone-pair interaction. Then it reaches an unstable intermediate **D**, where the nitrogen regains the tetrahedral geometry and the O–R′ bond is almost antiperiplanar to the nitrogen lone-pair. The intermediate **D** corresponds to the unstable intermediate **B** in Scheme 2. Partial rotation of the N–O bond results in the enantiomeric ground state conformation $\bar{\mathbf{A}}$. In "R-passing," the rate-determining transition state may be something like **TSR** in Fig. 6, where the alkyl group R eclipses a benzene ring, the nitrogen is planar, and the O–R′ bond is periplanar to the nitrogen lone-pair. The intermediate **E** is equivalent to **D** in "O-passing".

The energy of the ground state **A** will be higher when R′ = alkyl (**3**, **4**, **6**, and **7**) than when R′ = H (**2** and **5**) because of the steric interaction between R′ and the near-by benzene ring. The energy of the transition state for "O-passing" (**TSO**) will be rather similar irrespective of R′, because R′ does not sterically interact with the Tp skeleton. Thus the "O-passing" barrier will be lower when R′ = alkyl than when R′ = H. On the contrary, the energy of the transition state for "R-passing" (**TSR**) will be more dependent on the size of R′ than that of the ground state **A**, because R′ approaches the near-by benzene ring upon going from **A** to **TSR**. Thus the "R-passing" barrier will be higher when R′ = alkyl than when R′ = H. These predictions actually coincide with the observed features (a) and (c) mentioned above.

The feature (d) may also be ascribed mainly to the difference in the ground state energies. The methyl group in the *N*-ethyl group is tilted toward the near-by benzene ring, as revealed by the NOE experiments, and this would raise the ground state energy of the *N*-ethyl compounds relative to that of the corresponding *N*-methyl compounds, while the **TSR** energy will be rather similar between the *N*-ethyl and *N*-methyl compounds, because the methyl of the ethyl group will stand upright at **TSR**.

The higher "R-passing" barriers than the "O-passing" ones for the *N*,*O*-dialkyl compounds [the feature (e)] may be mainly ascribed to the larger eclipsing steric interaction of the benzene ring with the alkyl group R at the transition state **TSR** than with the oxy group OR′ at **TSO**. However, we do not at present have reasonable explanations for the similar and reversed barrier heights for **5** and **2**, respectively, and also for the feature (b).

In *N*-ethyl-*N*-methyl-9-triptycylamine (**8**), the "Me-passing" and "Et-passing" barriers have been found to be ca. 31 and 40 kJ mol^{-1}, respectively.[6] These values are significantly lower than the "R-passing" barriers found for **3**, **4**, **6**, and **7**. This will be interpreted as follows. These processes involve not only the eclipsing of the *N*-alkyl group with the benzene ring but also the nitrogen inversion. The barriers to nitrogen inversion in hydroxylamines are considerably higher than those in trialkylamines, mainly because of the unfavorable electrostatic interactions between the N- and O-lone pairs at the transition state; for example, 65.2 kJ mol^{-1} for *N*-methyl-1,2-oxazolidine (**9**)[11]

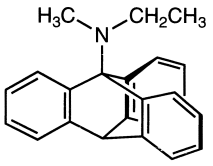

8

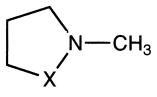

9: X = O
10: X = CH_2

Scheme 4.

vs 33 kJ mol^{-1} for *N*-methylpyrrolidine (**10**) (Scheme 4).[12]

In conclusion, the ground state structures of the *N*-9-triptycylhydroxylamines were revealed by X-ray crystallography and NMR spectroscopy, the stereomutation in solution was interpreted in terms of the passing of the *N*-substituents over the benzene rings of the triptycene skeleton, and their energy barriers were obtained by dynamic NMR studies.

Experimental

General. Melting points are not corrected. ^{1}H and ^{13}C NMR spectra were obtained on a Bruker ARX-300 spectrometer operating at 300.1 MHz for ^{1}H and 75.4 MHz for ^{13}C, respectively. Chemical shifts were referenced with internal tetramethylsilane (δ_H = 0) or $CDCl_3$ (δ_C = 77.0). Letters p, s, t, and q given with the ^{13}C chemical shifts denote primary, secondary, tertiary, and quaternary, respectively. In variable-temperature experiments, temperatures were calibrated using a methanol or an ethylene glycol sample and are reliable to ±1 °C.

***N*-9-Triptycylhydroxylamine (1).** To an ice-cold solution of 3.60 g (12 mmol) of 9-nitrotriptycene[10] in 400 mL of diethyl ether was added 1.82 g (48 mmol) of lithium tetrahydridoaluminate, and the mixture was heated under reflux for 30 min. After quenching with water, the mixture was extracted with dichloromethane. The extracts were washed with brine and dried over $MgSO_4$. After removal of the solvent, the residue was recrystallized from dichloromethane–hexane to afford 2.83 g (9.9 mmol, 83%) of **1**, mp 202–204 °C (Ref. 10, 198–199 °C). ^{1}H NMR ($CDCl_3$, 23 °C) δ 5.05 (1H, br s, OH), 5.35 (1H, s), 6.97–7.07 (6H, m), 7.12 (1H, br s, NH), 7.38 (3H, m), 7.57 (3H, m). ^{13}C NMR ($CDCl_3$, 23 °C) δ 53.7 (1C, t), 71.4 (1C, q), 121.4 (3C, t), 123.3 (3C, t), 125.0 (3C, t), 125.3 (3C, t), 143.9 (3C, q), 145.3 (3C, q). ^{1}H NMR (CD_2Cl_2, −90 °C) δ 5.59 (1H, s), 7.02–7.28 (6H, m), 7.32 (1H, br m, peri-H), 7.45–7.60 (4H, m, arom-H, NH), 7.88 (1H, br m, peri-H), 8.03 (1H, br m, peri-H), 8.21 (1H, br, OH).

***N*-Ethyl-*N*-9-triptycylhydroxylamine (2).** To an ice-cold solution of 1.71 g (6.0 mmol) of **1** in 80 mL of diethyl ether were added successively 0.48 mL (6 mmol) of pyridine and 3.9 mL (30 mmol) of ethyl trifluoromethanesulfonate, and the mixture was stirred for 2 h at 0 °C and 20 h at room temperature. The mixture was washed successively with aq $NaHCO_3$, water, and brine, and dried over $MgSO_4$. After evaporation of the solvent, the residue was chromatographed on a silica-gel column with hexane-dichloromethane as the eluent. Recrystallization from dichloromethane–hexane (2 : 1) gave 0.85 g (2.7 mmol, 45%) of **2** as colorless crystals, mp 219–220 °C. Found: C, 84.06; H, 6.10; N, 4.43%. Calcd for $C_{22}H_{19}NO$: C, 84.32; H, 6.11; N, 4.47%. ^{1}H NMR ($CDCl_3$, 23 °C) δ 1.61 (3H, t, J = 7.2 Hz), 4.02 (2H, q, J = 7.2 Hz), 5.27 (1H, s), 5.84 (1H, br), 6.94–7.04 (6H, m), 7.36 (3H, m), 7.69 (3H, br). ^{13}C NMR ($CDCl_3$, 23 °C) δ 14.4 (1C, p), 51.0 (1C, s), 54.5 (1C, t), 77.9 (1C, q), 123.4 (3C, t), 123.8 (3C, t, br), 124.6 (3C, t), 125.1 (3C, t), 144.0 (3C, q, br), 145.9 (3C, q). IR ($CDCl_3$) 3580 cm^{-1}. ^{1}H NMR (CD_2Cl_2, −72 °C) δ 1.61 (3H, t, J

= 7 Hz), 3.81 (1H, dq, J = 14 and 7 Hz), 4.13 (1H, dq, J = 14 and 7 Hz), 5.41 (1H, s), 6.38 (1H, br s, OH), 6.97 (1H, t, J = 7.4 Hz), 7.00–7.20 (5H, m), 7.28 (1H, m), 7.36 (1H, d, J = 7.3 Hz), 7.44 (1H, m), 7.55 (1H, m), 7.63 (1H, d, J = 7.3 Hz), 8.14 (1H, m).

***N*-Ethyl-*O*-methyl-*N*-9-triptycylhydroxylamine (3).** To an ice-cold solution of 313 mg (1.0 mmol) of **2** in 20 mL of diethyl ether were added 0.69 mL (1.1 mmol) of a 1.6 M solution of butyllithium in hexane and then 0.14 mL (1.2 mmol) of methyl trifluoromethanesulfonate. The mixture was stirred for 1 h at 0 °C and 2 h at room temperature. The mixture was washed successively with aq $NaHCO_3$, water, and brine, and dried over $MgSO_4$. Preparative TLC (silica gel) with dichloromethane–hexane (3 : 2) followed by recrystallization from dichloromethane–hexane (1 : 2) gave 45 mg (0.14 mmol, 14%) of **3**, mp 275–277 °C. Found: C, 84.08; H, 6.55; N, 4.38%. Calcd for $C_{23}H_{21}NO$: C, 84.37; H, 6.46; N, 4.28%. ^{1}H NMR ($CDCl_3$, 23 °C) δ 1.80 (3H, t, J = 7.2 Hz), 4.08 (2H, q, J = 7.2 Hz), 4.20 (3H, s), 5.24 (1H, s), 6.94–7.04 (6H, m), 7.34 (3H, m), 7.67 (3H, br d, J = 7 Hz). ^{13}C NMR ($CDCl_3$, 23 °C) δ 18.3 (1C, p), 52.8 (1C, s), 54.5 (1C, t), 63.6 (1C, p), 79.7 (1C, q), 123.2 (3C, t), 124.0 (3C, t, br), 124.5 (3C, t), 124.9 (3C, t), 144.5 (3C, q, br), 145.8 (3C, q). ^{1}H NMR (CD_2Cl_2, −75 °C) δ 1.81 (3H, t, J = 7 Hz), 3.86 (1H, dq, J = 14 and 7 Hz), 4.18 (3H, s), 4.26 (1H, dq, J = 14 and 7 Hz), 5.40 (1H, s), 6.98 (1H, t, J = 7.5 Hz), 7.00–7.15 (5H, m), 7.36 (1H, d, J = 6 Hz), 7.39 (1H, m), 7.42 (1H, m), 7.47–7.55 (2H, m), 8.08 (1H, m).

***N*,*O*-Diethyl-*N*-9-triptycylhydroxylamine (4).** To an ice-cold solution of 628 mg (2.0 mmol) of **2** in 20 mL of diethyl ether were added 1.58 mL (2.5 mmol) of a 1.6 M solution of butyllithium in hexane and then 0.52 mL (4 mmol) of ethyl trifluoromethanesulfonate. The mixture was stirred for 0.5 h at 0 °C and 4 h at room temperature. The mixture was washed successively with aq $NaHCO_3$, water, and brine, and dried over $MgSO_4$. Column chromatography on silica gel with dichloromethane as the eluent followed by recrystallization from dichloromethane–hexane (1 : 3) gave 150 mg (0.44 mmol, 22%) of **4**, mp 202–204 °C. Found: C, 84.43; H, 6.70; N, 4.19%. Calcd for $C_{24}H_{23}NO$: C, 84.42; H, 6.79; N, 4.10%. ^{1}H NMR ($CDCl_3$, 23 °C) δ 1.29 (3H, t, J = 7.2 Hz), 1.78 (3H, t, J = 7.2 Hz), 4.06 (2H, q, J = 7.2 Hz), 4.49 (2H, q, J = 7.2 Hz), 5.24 (1H, s), 6.94–7.03 (6H, m), 7.34 (3H, m), 7.67 (3H, br d, J = 7 Hz). ^{13}C NMR ($CDCl_3$, 23 °C) δ 14.4 (1C, p), 18.4 (1C, p), 53.2 (1C, s), 54.5 (1C, t), 70.6 (1C, s), 79.7 (1C, q), 123.2 (3C, t), 124.1 (3C, t, br), 124.5 (3C, t), 124.8 (3C, t), 144.4 (3C, q. br), 145.9 (3C, q). ^{1}H NMR (CD_2Cl_2, −69 °C) δ 1.23 (3H, t, J = 7 Hz), 1.79 (3H, t, J = 7 Hz), 3.85 (1H, dq, J = 14 and 7 Hz), 4.25 (1H, dq, J = 14 and 7 Hz), 4.35 (1H, dq, J = 8 and 7 Hz), 4.60 (1H, dq, J = 8 and 7 Hz), 5.38 (1H, s), 6.95–7.20 (6H, m), 7.30–7.42 (4H, m), 7.50 (1H, d, J = 6 Hz), 8.12 (1H, d, J = 6.4 Hz).

***N*-Methyl-*N*-9-triptycylhydroxylamine (5).** To an ice-cold solution of 1.71 g (6.0 mmol) of **1** in 80 mL of diethyl ether were added successively 0.48 mL (6 mmol) of pyridine and 3.4 mL (30 mmol) of methyl trifluoromethanesulfonate, and the mixture was stirred for 2 h at 0 °C and 24 h at room temperature. The mixture was washed successively with aq $NaHCO_3$, water, and brine, and dried over $MgSO_4$. After evaporation of the solvent, the residue was chromatographed on an alumina column with hexane-dichloromethane as the eluent. Recrystallization from dichloromethane–hexane (1 : 1) gave 0.85 g (2.8 mmol, 47%) of **2** as colorless crystals, mp 183–184 °C. Found: C, 84.11; H, 5.72; N, 4.67%. Calcd for $C_{21}H_{17}NO$: C, 84.25; H, 5.72; N, 4.68%. ^{1}H NMR ($CDCl_3$, 23 °C) δ 3.82 (3H, s), 5.28 (1H, s), 5.87 (1H, br s), 6.95–7.06 (6H, m), 7.38 (3H, m), 7.71 (3H, br). ^{13}C NMR ($CDCl_3$, 23 °C) δ 47.1 (1C, p), 54.4 (1C, t), 78.7 (1C, q), 123.5 (3C, t), 123.8 (3C, t, br), 124.6 (3C, t), 125.1 (3C, t), 143.6 (3C, q, br), 146.0 (3C, q). IR ($CDCl_3$) 3580 cm^{-1}. ^{1}H NMR (CD_2Cl_2, −64 °C) δ 3.83 (3H, s), 5.42 (1H, s), 6.95–7.20 (7H, m, arom-H, OH), 7.37 (1H, dd, J = 7 and 1 Hz), 7.41–7.49 (2H, m, H^B, arom-H), 7.56 (1H, m), 7.74 (1H, d, J = 7 Hz, H^A), 8.14 (1H, m, H^C).

***N*,*O*-Dimethyl-*N*-9-triptycylhydroxylamine (6).** To an ice-cold solution of 299 mg (1.0 mmol) of **5** in 20 mL of diethyl ether were added a suspension of 0.45 g (4 mmol) of KO^{t}Bu in 20 mL of diethyl ether and then 1.13 mL (10 mmol) of methyl trifluoromethanesulfonate. The mixture was stirred for 2 h at 0 °C and 2 h at room temperature. The mixture was washed successively with aq $NaHCO_3$, water, and brine, and dried over $MgSO_4$. Preparative TLC (silica gel) with dichloromethane–hexane (3 : 2) followed by recrystallization from dichloromethane–hexane (1 : 8) gave 42 mg (0.13 mmol, 13%) of **6**, mp 220–221 °C. Found: C, 84.02; H, 6.20; N, 4.47%. Calcd for $C_{22}H_{19}NO$: C, 84.32; H, 6.11; N, 4.47%. ^{1}H NMR ($CDCl_3$, 23 °C) δ 3.71 (3H, s), 4.01 (3H, s), 5.26 (1H, s), 6.98–7.04 (6H, m), 7.53 (3H, br), 7.66 (3H, br). ^{13}C NMR ($CDCl_3$, 23 °C) δ 43.2 (1C, p), 54.4 (1C, t), 59.3 (1C, p), 78.9 (1C, q), 123.2 (3C, t, br), 124.6 (3C, t, br), 125.0 (3C, t, br), 145.2 (3C, q, br) [Two aromatic peaks are too broad to be detected]. ^{1}H NMR (CD_2Cl_2, −68 °C) δ 3.70 (3H, s), 3.99 (3H, s), 5.41 (1H, s), 6.98 (1H, dt, J = 7.4 and 1.0 Hz), 7.00–7.20 (5H, m), 7.32–7.40 (2H, m), 7,43 (1H, m), 7.48 (1H, d, J = 7.5 Hz), 7.52 (1H, m), 8.04 (1H, m).

***O*-Ethyl-*N*-methyl-*N*-9-triptycylhydroxylamine (7).** To an ice-cold solution of 299 mg (1.0 mmol) of **2** in 20 mL of diethyl ether were added a suspension of 0.34 g (3 mmol) of KO^{t}Bu in 20 mL of diethyl ether and then 1.30 mL (10 mmol) of ethyl trifluoromethanesulfonate. The mixture was stirred for 2 h at 0 °C and 2 h at room temperature. The mixture was washed successively with aq $NaHCO_3$, water, and brine, and dried over $MgSO_4$. Preparative TLC (silica gel) with dichloromethane–hexane (3 : 2) followed by recrystallization from dichloromethane–hexane (1 : 8) gave 104 mg (0.32 mmol, 32%) of **7**, mp 206–208 °C. Found: C, 84.07; H, 6.52; N, 4.31%. Calcd for $C_{23}H_{21}NO$: C, 84.37; H, 6.46; N, 4.28%. ^{1}H NMR ($CDCl_3$, 23 °C) δ 1.32 (3H, t, J = 7.1 Hz), 3.70 (3H, s), 4.30 (2H, q, J = 7.1 Hz), 5.25 (1H, s), 6.90–7.04 (6H, m), 7.34 (3H, br), 7.66 (3H, br). ^{13}C NMR ($CDCl_3$, 23 °C) δ 14.0 (1C, p), 44.1 (1C, p), 54.4 (1C, t), 67.1 (1C, s), 78.8 (1C, q), 123.2 (3C, t, br), 124.5 (3C, t, br), 124.9 (3C, t, br), 145.9 (3C, q, br) [Two aromatic peaks are too broad to be detected]. ^{1}H NMR (CD_2Cl_2, −74 °C) δ 1.29 (3H, t, J = 7.1 Hz), 3.71 (3H, s), 4.22 (1H, dq, J = 8.2 and 7.1 Hz), 4.38 (1H, dq, J = 8.2 and 7.1 Hz), 5.42 (1H, s), 7.03–7.18 (6H, m), 7.33–7.47 (4H, m), 7.53 (1H, m), 8.09 (1H, m).

Lineshape Analysis. Total lineshape analysis was performed by visual matching of experimental spectra with theoretical spectra computed on an NEC PC9821Xs personal computer equipped with a Mutoh PP-210 plotter using the DNMR3K program, a modified version of the DNMR3 program[13] converted for use on personal computers by Dr. Hiroshi Kihara. Temperature dependences of chemical shift differences and T_2 values were properly taken into account.

X-ray Crystallography. Crystals of compound **4** were grown from dichloromethane-hexane. The crystal data, the parameters for data collection, structure determination, and refinement are summarized in Table 3. Diffraction data were collected on a Rigaku AFC7R diffractometer and calculations were performed using the SHELXL93 program.[14] The structure was solved by direct methods, followed by full-matrix least-squares refinement

Table 3. Crystal Data of Compound **4**, Parameters for Data Collection, Structure Determination, and Refinement

Empirical formula	$(C_{24}H_{23}NO)_2$
Formula weight	682.87
Crystal system	triclinic
Space group	$P\bar{1}$
a (Å)	13.583 (3)
b (Å)	15.575 (5)
c (Å)	8.954 (3)
α (°)	91.45 (3)
β (°)	90.20 (2)
γ (°)	101.71 (2)
V (Å^3)	1854.2 (9)
Z	2
D_c (g cm^{-3})	1.223
F(000)	728
μ(Mo-K$_\alpha$) (cm^{-1})	0.074
Temp (°C)	20 ± 2
$2\theta_{max}$ (°)	55.0
No. of reflections measured	
Total	8520
Unique	6296
No. of refinement variables	653
Final R ; R_w	0.050; 0.127
GOF	1.07

$R = \Sigma||F_o|-|F_c||/\Sigma|F_o|$, R_w on F^2.

with all non-hydrogen atoms anisotropic and hydrogen atoms isotropic. Reflection data with $|I| > 2.0\sigma(I)$ were used. The function minimized was $\Sigma w(|F_o|-|F_c|)^2$ where $w = [\sigma^2(F_o)]^{-1}$.

Crystallographic data have been deposited at the CCDC, 12 Union Road, Cambridge, CB2 1EZ, UK and copies can be obtained on request, free of charge, by quoting the publication citation and the deposition number 162324, and the final atomic parameters and structure factors have been deposited as Document No. 74041 at the Office of the Editor of Bull. Chem. Soc. Jpn.

Molecular Mechanics Studies. Molecular mechanics calculations were performed employing the MM3 program[15] with the 1989 force field on an NEC EWS-4800/360 work station. The following parameters were added: 6–8: l_o = 1.440 Å, k_s = 5.00 md Å^{-1}, bond moment = 0; 1–6–8: θ_o = 104.0°, k_s = 0.42 md Å rad^{-2} ; 8–6–28: θ_o = 104.0°, k_s = 0.42 md Å rad^{-2}; 1–8–6: θ_o = 105.5°, k_s = 0.74 md Å rad^{-2}. All the torsional parameters x–6–8–y were set to zero. These values were chosen after consulting the existing parameters in the force field and might be inadequate.

References

1 M. Raban and D. Kost, in "Acyclic Organonitrogen Stereodynamics," ed by J. B. Lambert and Y. Takeuchi, VCH Publishers, New York (1992), Chap. 2.

2 F. G. Riddell, *Tetrahedron*, **37**, 849 (1981).

3 M. Raban and D. Kost, *Tetrahedron*, **40**, 3345 (1984).

4 The oxygen lone pairs may be assumed to reside in two sp^3-hybridized orbitals, or one in an s-type and the other in a p-type orbital.

5 See for example: M. Ōki, "The Chemistry of Rotational Isomers," Springer Verlag, Berlin (1993); M. Ōki, *Acc. Chem. Res.*, **23**, 351 (1990).

6 G. Yamamoto, H. Higuchi, M. Yonebayashi, and J. Ojima, *Chem. Lett.*, **1994**, 1911; G. Yamamoto, H. Higuchi, M. Yonebayashi, Y. Nabeta, and J. Ojima, *Tetrahedron*, **52**, 12409 (1996).

7 G. Yamamoto, H. Higuchi, M. Yonebayashi, Y. Nabeta, and J. Ojima, *Chem. Lett.*, **1995**, 853; G. Yamamoto, K. Inoue, H. Higuchi, M. Yonebayashi, Y. Nabeta, and J. Ojima, *Bull. Chem. Soc. Jpn.*, **71**, 1241 (1998).

8 G. Yamamoto, H. Murakami, N. Tsubai, and Y. Mazaki, *Chem. Lett.*, **1997**, 605; G. Yamamoto, N. Tsubai, H. Murakami, and Y. Mazaki, *Chem. Lett.*, **1997**, 1295; G. Yamamoto, F. Nakajo, N. Tsubai, H. Murakami, and Y. Mazaki, *Bull. Chem. Soc. Jpn.*, **72**, 2315 (1999) .

9 A part of the results has been reported in a preliminary form: G. Yamamoto, F. Nakajo, N. Endo, and Y. Mazaki, *Chem. Lett.*, **2000**, 1102.

10 W. Theilacker and K.-H. Beyer, *Chem. Ber.*, **94**, 2968 (1961).

11 F. G. Riddell, J. M. Lehn, and J. Wagner, *J. Chem. Soc., Chem. Commun.*, **1968**, 1403.

12 J. M. Lehn and J. Wagner, *Tetrahedron*, **26**, 4227 (1970).

13 D. A. Kleier and G. Binsch, QCPE Program No. 165.

14 G. M. Sheldrick, Program for the Refinement of Crystal Structures. University of Göttingen, Germany (1993).

15 The program was obtained from Technical Utilization Corporation.